ELSEVIER

Biochimica et Biophysica Acta 1415 (1998) 23–40

BIOCHIMICA ET BIOPHYSICA ACTA
BBA

Doxorubicin physical state in solution and inside liposomes loaded via a pH gradient

Xingong Li [a], Donald J. Hirsh [a], Donna Cabral-Lilly [a], Achim Zirkel [b], Sol M. Gruner [b], Andrew S. Janoff [a], Walter R. Perkins [a,*]

[a] *The Liposome Company, Inc., One Research Way, Princeton, NJ 08540, USA*
[b] *Department of Physics, Cornell University, Ithaca, NY 14853, USA*

Received 26 May 1998; accepted 9 September 1998

Abstract

We have examined doxorubicin's (DOX) physical state in solution and inside EPC/cholesterol liposomes that were loaded via a transmembrane pH gradient. Using cryogenic electron microscopy (cryo-EM) we noted that DOX loaded to 200–300 mM internal concentrations in citrate containing liposomes formed linear, curved, and circular bundles of fibers with no significant interaction/perturbation of the vesicle membrane. The individual DOX fibers are putatively comprised of stacked DOX molecules. From end-on views of bundles of fibers it appeared that they are aligned longitudinally in a hexagonal array with a separation between fibers of approx. 3–3.5 nm. Two distinct small angle X-ray diffraction patterns (oblique and simple hexagonal) were observed for DOX-citrate fiber aggregates that had been concentrated from solution at either pH 4 or 5. The doxorubicin fibers were also present in citrate liposomes loaded with only one-tenth the amount of doxorubicin used above (approx. 20 mM internal DOX concentration) indicating that the threshold concentration at which these structures form is relatively low. In fact, from cryo-EM and circular dichroism spectra, we estimate that the DOX-citrate fiber bundles can account for the vast majority ($>99\%$) of DOX loaded via a pH gradient into citrate buffered liposomes. DOX loaded into liposomes containing lactobionic acid (LBA), a monoanionic buffer to control the internal pH, remained disaggregated at internal DOX concentrations of approx. 20 mM but formed uncondensed fibers (no bundles) when the internal DOX concentration was approx. 200 mM. This finding suggests that in the citrate containing liposomes the citrate multianion electrostatically bridged adjacent fibers to form the observed bundles. ^{13}C-NMR measurements of [1,5-^{13}C]citrate inside liposomes suggested that citrate 'bound' to the DOX complex and 'free' citrate rapidly exchange indicating that the citrate-DOX interaction is quite dynamic. DOX release into buffer was relatively slow ($<4\%$ at 1 h) from liposomes containing DOX fibers (in citrate loaded to a low or high DOX concentration or in LBA liposomes loaded to a high internal DOX concentration). LBA containing liposomes loaded with disaggregated DOX, where the internal DOX concentration was only approx. 20 mM, experienced an osmotic stress induced vesicle rupture with as much as 18% DOX leakage in less than 10 min. The possible implications for this in vivo are discussed.

Keywords: Adriamycin; Remote loading; Cryo-electron microscopy; TLC D-99; Evacet

Abbreviations: CD, circular dichroism; cryo-EM, cryogenic electron microscopy; DOX, doxorubicin; EPC, egg phosphatidylcholine; HBS, HEPES buffered saline; LBA, lactobionic acid; LUV, large unilamellar vesicle; MLV, multilamellar vesicle; NMR, nuclear magnetic resonance; SAXS, small angle X-ray diffraction

* Corresponding author. Fax: (609) 520-8250; E-mail: wperkins@lipo.com

0005-2736/98/$ – see front matter
PII: S0005-2736(98)00175-8

1. Introduction

The major limitation of doxorubicin (DOX), one of the most widely used anticancer agents, has been its cumulative dose related cardiotoxicity [1]. Liposome encapsulation has been shown to reduce the cardiotoxicity of anthracyclines in animal models [2–5] and one formulation of liposomal DOX (Evacet, formerly TLC D-99) has been shown to be less cardiotoxic in humans [6]. In this formulation, encapsulation has been made highly efficient ($>95\%$) by taking advantage of DOX's accumulation to the liposome interior in response to an inside-acidic transmembrane pH gradient. The encapsulation procedure has been referred to as remote loading [7–9].

Transmembrane pH gradients can be created directly, as in the above case, by forming the liposomes in a well-buffered solution of low pH (e.g., 300 mM citrate at pH 4) and then adding a more basic solution to raise the external solution pH [7]. pH gradients can also be created indirectly by an electrical potential which drives protons to the vesicle interior [8] or from the electroneutral outward flow of the counterion to an entrapped acid (e.g., ammonium sulfate [9]). With a pH gradient established, DOX accumulates in the vesicle interior and the ideal distribution of DOX in solution inside (D_{in}) and outside (D_{out}) the liposomes is expected to be related to the inner and outer H^+ concentrations by

$$\frac{D_{in}}{D_{out}} = \frac{V_{in}}{V_{out}}\left(\frac{K + [H^+]_{in}}{K + [H^+]_{out}}\right) \quad (1)$$

where V_{in} and V_{out} are the internal and external aqueous volumes and K is the dissociation constant for DOX ($pK = 8.22$ [10]). However, we and others [11] have found that D_{in}/D_{out} can exceed the value predicted by Eq. 1. One explanation for this enhanced accumulation is that internalized DOX does not remain in solution. Precipitation of DOX, for example, from the internal solution would facilitate movement of additional DOX from the outside to satisfy the equilibrium relationship of Eq. 1. In fact, Lasic et al. [12,13], employing an ammonium sulfate gradient to load DOX into liposomes, have shown that in these systems internalized DOX forms aggregates. Using cryo-electron microscopy, they were able to visualize the internalized DOX aggregates and found structures similar to those caused by precipitation of DOX with sulfate anion in solution.

Aggregation could also explain the restriction of DOX molecular motions noted by Cullis and co-workers who studied DOX entrapped by a transmembrane pH gradient into citrate containing liposomes. Although Cullis and co-workers have suggested that citrate could cause precipitation of this internalized DOX [7,11], in more recent work they have proposed that the attenuation of the DOX nuclear magnetic resonance (NMR) signal they observed was due entirely to its binding to the liposome's inner surface [14]. Moreover, in order to explain the internalized structures they observed inside DOX liposomes by cryo-electron microscopy [15] they proposed that DOX produces invagination of the liposome bilayer membrane. Because images of these liposomes were similar in appearance to those containing DOX-sulfate aggregates [13] and because we have noted that DOX forms a precipitate in citrate solutions, we believed the nature of DOX's physical state in citrate bearing liposomes to remain in question.

It was our desire here to study in detail the physical state of DOX inside citrate containing liposomes. We examined DOX in solution and inside liposomes by various methods and found that DOX can form highly organized bundles of fibrous structures in the presence of citrate. Our results indicate that $>99\%$ of DOX internalized in liposomes at 20–300 mM is predominantly self-associated and not bound to the inner membrane surface.

To assess the extent to which counterion valency influences DOX organization, we also examined liposomes in which the monoanionic compound lactobionic acid (LBA) was used to buffer the vesicle interior. When a pH gradient was established and these systems were loaded with DOX (approx. 200 mM DOX inside liposomes), fibrous structures were observed, but unlike the structures we found in citrate liposomes these fibers were disorganized and not condensed into bundles. When these systems were loaded with low internal DOX concentrations no fibers were observed. Whether in this case DOX was bound to the liposome inner surface remains unclear, but membrane invagination did not occur.

Because the physical state of DOX inside liposomes could be manipulated, we ventured to examine

its impact upon release. Leak profiles were not distinguishable for DOX loaded at high internal concentrations (approx. 200 mM DOX) into either citrate or LBA containing liposomes. For DOX loaded to low internal concentrations (approx. 20 mM DOX) where DOX was either in fiber bundles (citrate) or disaggregated (LBA), different leak rates were noted. However, we found this difference to be due to an osmotic stress related rupture for the LBA liposomes. When osmotic stress was avoided the leak profiles were similar. Because in the LBA liposomes DOX was disaggregated at the low DOX concentration, we speculate that fiber formation may play an important role in curtailing DOX loss in vivo, an important concern considering the long residence time that DOX liposomes have in the circulation [16] and the fact that plasma constituents increase liposome leak [17].

2. Materials and methods

2.1. Materials

Egg phosphatidylcholine (EPC) and cholesterol were obtained from Avanti Polar Lipids (Alasbaster, AL). DOX-HCl (Adriamycin RDF) was purchased from Farmitalia Carlo Erba (Milan, Italy). For NMR, DOX from Sigma (St. Louis, MO) was used. Citric acid monohydrate, ammonium sulfate, chromiumoxalate (trihydrate) (potassium salt), 4-oxo-TEMPO (TEMPONE) and 4-amino-TEMPO were obtained from Aldrich (Milwaukee, WI). [1,5-^{13}C]Citrate was purchased from Isotec (Miamisburg, OH). HEPES, cholesterol calibrator, and cholesterol diagnostic kits were purchased from Sigma. Octaethylene glycol monododecyl ether (C12E8) was obtained from Fluka (Buchs, Switzerland). Tetra(sulfonatophenyl)porphine was purchased from Porphyrin Products (Logan, UT). Sodium carbonate anhydrous was purchased from J.T. Baker (Phillipsburg, NJ). All the chemicals used were the highest purity available.

2.2. Liposome preparation and lipid assay

Liposomes were made by extrusion of lipid suspensions first made by solvent evaporation. These structures were used instead of multilamellar vesicles (MLVs) because we wanted to avoid localized solute exclusion [18,19]. Freezing and thawing the MLVs would not have attained an ideal solute distribution because the high concentration of solutes used here afforded these systems cryoprotection. For the initial liposome suspensions, chloroform stock solutions of EPC and cholesterol (approx. 20 mg/ml lipid) were mixed at 55:45 (mole) ratio, accordingly. After adding 2.5 ml of either 300 mM citric acid (pH 4.0) or 650 mM lactobionic acid (pH 3.6) into the chloroform mixture (approx. 25 ml), the chloroform was removed by rotary evaporation at 40°C. When essentially all of the chloroform was judged to be removed an additional 2.5 ml of the appropriate buffer was added to the paste that had formed and the sample was subjected to further rotary evaporation at 40°C. If necessary, the resulting suspensions were then adjusted with distilled water to a total volume of 5 ml. These liposomes were then extruded through two stacked filters of pore size 400 nm (one pass) and then 200 nm (ten passes) at 40°C; filters were polycarbonate Nuclepore membranes from Nuclepore Corporation (Pleasanton, CA). Liposome size was determined by light scattering using a Nicomp Model 270/370 Submicron Particle Sizer from Pacific Scientific (Menlo Park, CA).

The phospholipid concentration of all liposome samples was measured by a modified version of the procedure of Chen et al. [20]. Cholesterol concentrations were determined using the cholesterol diagnostic kit from Sigma. Absorbances were recorded on an UV-2101PC UV-scanning spectrophotometer from Shimadzu Scientific Instruments (Princeton, NJ).

2.3. Doxorubicin loading and leak assays

2.3.1. Loading of DOX into liposomes

Unless stated otherwise transmembrane pH gradients were created by adding an aliquot of sodium carbonate solution (17.6 mg/ml) into the liposome samples. The pH of the aqueous solution outside the liposomes ranged from 7.8 to 8.1. This liposome suspension was then mixed with a DOX saline solution. The final overall DOX concentration was either 3.4 mM or 0.34 mM, whereas the lipid concentration was approx. 12.8 mM. An aliquot of 10 mM 4-amino-TEMPO was added if the pH gradient

across the lipid bilayer was to be measured. To accelerate loading, the sample was then heated to 55–60°C for 10 min and cooled to room temperature.

The loading efficiency was determined using gel chromatography to remove unencapsulated material. Aliquots of each sample were passed down columns pre-equilibrated with 10 mM HEPES, 150 mM NaCl (HBS) at pH 7.5. The liposome fraction was gathered and this material and an aliquot not passed down the column were adjusted to an equivalent volume with saline and then assayed for lipid by phosphate analysis. Each sample was also assayed for DOX content by dissolution in methanol and measurement of the absorbance at 490 nm. The percent entrapment was calculated as that percent of DOX remaining with the liposomes following elution; DOX concentrations were normalized using the lipid concentrations.

For LBA, we found that 650 mM LBA maintained pH gradients (3 units) for several hours without any measurable decrease thus indicating that LBA's permeability to these liposome membranes is low; all subsequent experiments were performed well within this time frame. Additionally, 650 mM LBA allowed the complete loading of DOX at 3.4 mM DOX and 12.8 mM lipid. At 500 mM LBA, the buffer capacity was insufficient to achieve complete DOX loading.

2.3.2. Doxorubicin leakage from liposomes

To compare DOX leak from liposomes, an aliquot of liposomal DOX was diluted 300-fold by injection into a cuvette containing a solution of 10 mM HBS (pH 7.5). The fluorescence intensity of DOX was measured continually with data collected every 10 s. The excitation and emission wavelengths were 480 nm and 590 nm, respectively. At the end of each measurement, C12E8 was added to dissolve the liposomes and attain the 100% leakage value. The percentage of leakage of DOX from liposomes at a given time was calculated using Eq. 2:

$$\%\ \text{leakage} = \frac{(I - I_0)}{(I_{100} - I_0)} \times 100 \qquad (2)$$

where I was the fluorescence intensity at a given time and I_0 and I_{100} were intensities immediately after the initial dilution into HBS or after addition of C12E8, respectively. DOX fluorescence intensity (without liposomes) decreased linearly with time for samples maintained above pH 7, due to DOX degradation at higher pH values [10,21]. The magnitude of this decrease at pH 7 was small ($< 2\%$ per hour). Therefore, we did not adjust the leak equation to reflect this loss. At pH 4 no decrease in DOX fluorescence intensity was noted up to 7 h.

2.3.3. Measurement of ΔpH and captured volume

To measure internal pH, and thus ΔpH, we used the distribution of an electron spin resonance (ESR) amine probe [22]. The ESR probe 4-amino-TEMPO was added to liposomes at the time of DOX loading (final concentration 200 μM). The sample was separated into fractions and these fractions were then diluted equally with either a solution of buffer (10 mM HBS at pH 7.5) alone or with buffer containing the broadening agent chromiumoxalate (trihydrate). The solution containing broadening agent was first adjusted to the same osmotic strength as that of the liposome solution to avoid vesicle shrinkage or swelling. All osmolarity measurements were performed with a 5500 Vapor Pressure Osmometer from Wescor (Logan, UT). The ESR spectra of both fractions were then recorded and the ΔpH was calculated using the following relationship:

$$\Delta\text{pH} = \log_{10}\left(\frac{A_{\text{in}}}{A_{\text{tot}} - A_{\text{in}}} \times \frac{V_{\text{out}}}{V_{\text{in}}}\right) \qquad (3)$$

where A_{in} and A_{tot} were the amplitudes of the ESR $I = +1$ resonance with and without the broadening agent, respectively. V_{in} and V_{out} were the aqueous volume inside and outside the liposomes, respectively. The values of V_{in} and V_{out} were obtained separately from the measurement of captured volume.

The captured volume of the liposomes was determined using an ESR procedure previously described [23] which is a slight modification of the method of Anasi et al. [24]. The ESR spin probe TEMPONE (in the appropriate buffer) was added to the sample in question which had first been adjusted to pH 7–8 by addition of sodium carbonate (17.6 mg/ml) solution. Adjustment of the pH to above pH 5 was necessary to prevent leakage of the chromiumoxalate broadening agent that was to be added later. The liposome sample (38 mg/ml lipid) containing TEMPONE (1 mM) was separated into 100 μl fractions. To one fraction the same liposome buffer solution (100 μl) was added and to another faction the chromiumoxalate broadening agent solution (100 μl) was added.

The ESR signal amplitudes with and without broadening agent were then related to the inside and total aqueous volumes, respectively. Captured volume (μl/μmole lipid) was then derived as previously described using a correction to account for the volume occupied by the lipid [23].

2.4. Microscopy

For confocal microscopy, fluorescence images were acquired with a Biorad 1000 Confocal Microscope from Olympus (Hercules, CA), using a Kr/Ar laser with λ_{ex} at 568 nm and λ_{em} at 605 nm. For cryo-electron microscopy, frozen-hydrated samples were prepared by placing 5 μl of a liposomal suspension on a copper grid with a holey carbon support. Each sample was blotted to a thin film and immediately plunged into liquid ethane. The grids were then stored under liquid nitrogen until used. The grids were viewed on a Philips CM12 transmission electron microscope (Mahwah, NJ) operating at an accelerating voltage of 120 kV. The microscope was equipped with a Gatan 626 cryoholder (Warrendale, PA), and the samples were maintained at −177°C during imaging. Electron micrographs were recorded under low electron dose conditions at a magnification of 60 000× and 1.4–1.7 μm defocus.

2.5. X-Ray diffraction

Solution aggregates for X-ray diffraction were prepared by mixing equal parts of a solution of DOX (15 mg/ml) and 600 mM (final conc. 300 mM) citrate at the appropriate pH. Aggregates immediately formed and after 10 min the samples were concentrated via centrifugation (14 000×g) and the supernatant removed. For the heated samples, after aggregate formation the samples were heated to 55–60°C and cooled back to room temperature prior to concentration via centrifugation. For liposomes containing DOX, loaded liposomes and empty liposomes (to correct for liposome scattering) were pelleted via centrifugation at 210 000×g for 2 h. Pelleted samples were placed in 1.5 mm diameter glass X-ray capillaries which were then flame sealed. X-Rays were produced by a Rigaku RU-200 rotating anode generator at a typical loading of 40 kV and 60 mA. The Cu Kα line at 1.54 Å was selected and focused by Ni filtering and double mirror Franks optics, which resulted in a typical flux at the sampled of 7×10^7 X-rays/s. The sample temperature stage was thermoelectrically adjusted to the desired temperature to within ±0.1°C. A two-dimensional X-ray detector based on a 512×512 pixel Thomson CCD [25] was used to acquire the data. The diffraction patterns were concentric powder pattern rings which were azimuthally integrated into one-dimensional plots of intensity versus scattering angle. Typical integrated exposures ranged from 20 to 60 min in duration.

Diffraction signals were analyzed over a q-range of 0.1–0.8 $Å^{-1}$, where the wave vector q is defined by

$$q = \frac{4\pi}{\lambda}\sin\left(\frac{\theta}{2}\right) \tag{4}$$

where θ is the scattering angle and λ is the wavelength of the incident radiation. Based on the cryo-EM data, we assumed that the X-rays basically probed only two dimensions of the structure with the third dimension (along the fiber's axis) being too large to be seen. The diffraction was analyzed in terms of a general oblique planar lattice in which the two unit cell basis vector lengths, a and b, are not constrained to have the same length and in which the smallest angle between them, $\gamma+\pi/2$, is constrained only in that $0<\gamma<\pi/2$. The general formula in two dimensions for the peak positions in reciprocal space with Miller indices h, k is given by:

$$\frac{q^2}{(2\pi)^2} = \frac{h^2}{a^2\sin^2\gamma} + \frac{2hk\cos\gamma}{ab\sin^2\gamma} + \frac{k^2}{b^2\sin^2\gamma} \tag{5}$$

2.6. Fluorescence and resonance light scattering

DOX fluorescence in solution was measured using an Alpha Scan Spectrofluorometer from PTI (South Brunswick, NJ). Excitation and emission wavelengths were set at 480 nm and 590 nm, respectively. For resonance light scattering measurements, excitation and emission wavelengths were kept identical as the spectrum was scanned from 200 nm to 900 nm; this is essentially a ∠90° light scattering experiment as a function of wavelength (see Pasternack et al. [26,27] for details). Tetra(sulfonatophenyl)porphine at pH 1 was used as a positive control for RLS (R. Pasternack, personal communication).

2.7. Spectrophotometric assays

2.7.1. Circular dichroism (CD) spectroscopy

Liposomal DOX suspensions, or DOX aqueous solutions/suspensions containing saline, water, citrate, or lactobionic acid were typically placed in a 1 mm CD cell. The CD spectra were taken at room temperature (20–23°C) from 700 nm to 200 nm on a J-710 spectropolarimeter (Jasco, Easton, MD) and typically the average of five scans was reported with removal of high frequency noise.

2.7.2. Turbidity and UV-Vis spectra measurement

The turbidity (absorbance) and UV-visible spectra of different DOX aqueous solutions/suspensions were measured using a 1 cm pathlength quartz cell in a UV-2101 Spectrophotometer from Shimadzu Scientific Instruments. For turbidity, absorbance was measured at 800 nm. This relatively high wavelength was chosen to avoid any interference from DOX absorption.

2.8. Differential scanning calorimetry (DSC)

Calorimetry was performed using a MC2 Ultrasensitive Scanning Calorimeter (MicroCal, Northhampton, MA). Heating scans were obtained from 15°C to 85°C at a rate of 20°C/h.

2.9. NMR spectroscopy

2.9.1. NMR sample preparation

For NMR samples, liposomes were prepared as described in Section 2.2 except that for citrate containing liposomes, [1,5-^{13}C]citrate was mixed with unlabeled citrate to give either 17 or 47 mole % [1,5-^{13}C]citrate. The final concentrations of citrate and LBA in which the liposomes were formed were 270 mM and 650 mM, respectively. To establish a pH gradient and to remove the outer buffer solutions, liposomes were passed down polyacrylamide columns (Pierce, Rockford, IL) equilibrated with 20 mM HBS at pH 7.6. Only the first 2/3 or so of the eluting liposomes were used so as to guarantee removal of as much external buffer as possible and the lipid concentration was then analyzed. DOX (from Sigma) was then hydrated with saline and then mixed with an aliquot of liposomes and additional HBS such that the final lipid concentration was 12.8 mM lipid and the final DOX concentrations were either 3.4 or 0.34 mM DOX (2 mg/ml or 0.2 mg/ml). Upon mixing, the liposomes were then heated to 55–60°C for 10 min. The samples were then examined by CD to confirm typical spectra and then used for NMR measurements. Samples were stored at approx. 5°C. The NMR signal of the citrate buffer alone was used to gauge the amount of citrate trapped inside the empty liposomes. This amount of citrate was approx. 6.2 mM (total solution concentration). At 3.4 mM overall DOX and assuming complete loading, this corresponds to a ratio of approx. 1.8 citrate molecules per DOX molecule in the liposome interior.

2.9.2. ^{13}C-NMR spectroscopy

Data were acquired on a Bruker AC 300 NMR spectrometer using a 10 mm broadband probe from Nalorac Cryogenics Corporation. The resonant frequency for ^{13}C was 75.5 MHz. Free induction decays (FIDs) were acquired with proton decoupling using a 20 kHz sweep width and 16K points. No internal field lock signal was used. Data for the T_1 measurements were acquired using the saturation-recovery method. Signal intensities (peak areas) were plotted versus time and fit by the equation: $I(t) = I(0)[1-\exp(-t/T_1)]$. Data for the T_2 measurements were collected with the Carr-Purcell-Meiboom-Gill pulse sequence. Where signal intensities of different samples were compared, the FIDs were collected using a 14.8 μs 90° pulse, a recycle delay $\geq 5 \times T_1$, and proton decoupling applied only during the data acquisition period. Other FIDs were collected with the minimum recycle delay allowed by the spectrometer and the pulse width set to the Ernst angle for the spins of interest. At the end of data acquisition for a particular sample, ethylene glycol, 0.2% v/v, was added as an internal chemical shift reference (64.0 ppm) and a final set of FIDs were summed. The Fourier transform of this data was used to assign the chemical shifts. Prior to Fourier transformation, all FIDs were zero-filled to 32K points and multiplied by an exponential decay corresponding to 3 Hz.

3. Results

To load DOX into liposomes, Cullis and co-workers have used transmembrane pH gradients ($pH_{in} \approx 4$, $pH_{out} \approx 7.5$) created using either citrate [7] or glutamate [28] to buffer the vesicle interior. This work was the basis for a liposomal DOX formulation (Evacet, formerly TLC D-99) that is currently being evaluated in clinical trials [29–31]. With this strategy, DOX can be loaded to high concentrations inside liposomes (200–300 mM internal concentrations). This is far in excess of DOX's solubility limit in solution, which is ≤60 mM in water [12]. The question then arises as to what physical structure does DOX adopt or does it bind to the inner monolayer of the liposome. The purpose of our study here was to investigate the physical state of DOX inside liposomes.

3.1. Doxorubicin in solution

As indicated in Table 1, the physical state of DOX in solution is clearly influenced by the valency of the counterion. When combined with the multianions citrate or sulfate, DOX formed a viscous gel which upon shaking yielded fibrous structures (Fig. 1). The resulting structures were similar in appearance to those previously reported for DOX-sulfate aggregates [9]. No such structures were observed for DOX in water or in solutions of glutamate or the monoanionic buffer lactobionic acid (LBA). Why glutamate, which has two carboxylic acid groups, did not initiate aggregate formation is unclear but it does also contain a cationic amine group which might obviate assemblage of the DOX structures electrostatically. Because we were interested in what happens to DOX inside citrate containing liposomes we focused our attention upon citrate-doxorubicin interactions for the remainder of the studies discussed here.

Table 1
Formation of DOX aggregates in solution

Counterion	pH	Aggregate formation	[DOX] at which aggregation begins[a] (mM)
Citrate	4–7	yes	0.5–1.5
Sulfate	4–7	yes	1.0
LBA	4	no	>20[b]
Glutamate	4	no	>20[b]

[a]Aggregation onset was measured by the increase in turbidity ($A_{800\,nm}$) of DOX at 4 mM in the indicated solutions.
[b]Determined visually not spectrophotometrically. DOX predissolved in water was mixed 1:1 with solutions. Final counterion concentrations were 300 mM for citrate, 650 mM for LBA, 110 mM for sulfate, and 175 mM for glutamate. These counterion concentrations were selected as they are the concentrations used previously with DOX liposomes.

The DOX-citrate structures we observed in solution were assembled into linear fibrous-like structures. Upon close inspection the larger strands were found to be bundles of smaller fibers, similar in appearance to micellar fibers resulting from porphyrin stacking/aggregation [32]. These fibrous structures disappeared upon heating and reappeared with cooling. Calorimetric scans of 4 mg/ml DOX in 300 mM citrate revealed a broad endotherm which was near 43°C at pH 4 but which was shifted upward to 57°C at pH 5; ΔH was 1.8 and 2.8 kcal/mole, respectively (data not shown). The melting of DOX-citrate precipitate may be similar to the 'melt' of hydrated micellar crystals (Krafft point) that has been described for local anesthetics [33,34]. An exothermic peak was also observed in the scans of both samples at approx. 75 and 65°C, respectively, which was absent upon subsequent heating cycles. A visual check of heated samples confirmed that disaggregation was associated with the endothermic transition and not the exothermic event. From TLC analysis, it appeared that the exothermic transition represented loss of DOX's amino sugar moiety (not shown). In the work we report here, samples in solution or in vesicles were never heated to beyond 60°C.

3.2. Cryo-EM of DOX inside citrate liposomes

Shown in Fig. 2 are cryo-EM images of citrate bearing liposomes loaded with DOX. In all cases DOX formed fibrous aggregates inside the liposomes and the liposome membranes (both inner and outer monolayers) were well resolved with no observable membrane invagination. The arrow in Fig. 2A points to an end-on view of a 'U'-shaped bundle of DOX fibers that are packed hexagonally. A similar U-shaped bundle is seen in profile in Fig. 2B. Fibrous DOX bundles were apparent in nearly all liposomes and were either linear, curved (some having a 'U'-

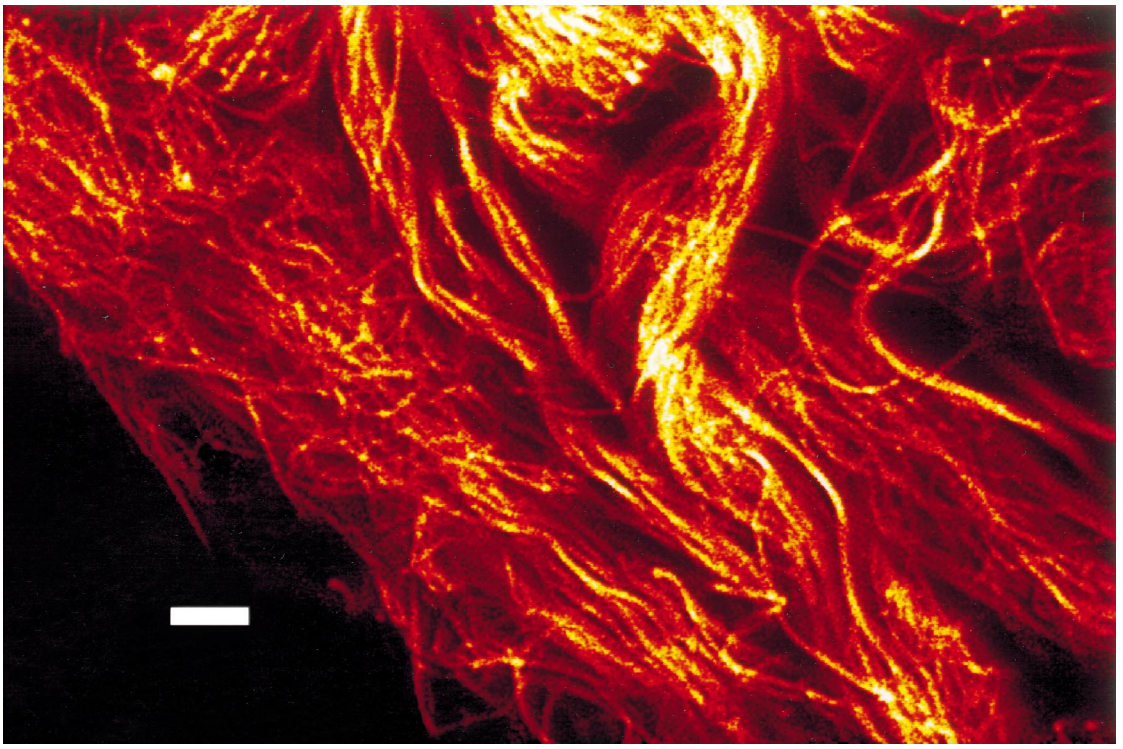

Fig. 1. Confocal light microscopy of DOX-citrate fibrous bundles. DOX in water was mixed 1:1 with a citrate solution for a final concentration of 4 mM DOX and 300 mM citrate at pH 4. Similar DOX aggregates were observed in solutions of citrate at pH 5 and ammonium sulfate at pH 4 and 7 (not shown). Image was colored to better visualize structures three-dimensionally. Bar length is 5 μm.

shape), or circular where the fibers apparently closed back upon themselves. For many of the longer linear DOX structures, liposomes were obviously elongated to accommodate fiber growth. Many of the bundles appeared to twist, as for example, the large circular structure in Fig. 2A. From the hexagonal pattern in Fig. 2A, the number of fibers in that particular bundle appeared to be approx. 50. This value would appear to vary since end-on views of other U-shaped structures (not shown) revealed a range of 12–60 fibers/bundle, all in a hexagonal arrangement. From this end-on perspective the average spacing between fibers was estimated to be 3–3.5 nm. In some cases, striations could be observed along the length of the bundles that alternated with non-striated regions. For example, the arrows in Fig. 2C indicate repeating striated regions in the DOX fibrous bundles. The distance between the centers of these striated regions appeared to be approx. 50 nm. Interestingly, measuring across the striations (perpendicular to bundle's long axis) we estimated that the striated 'lines' themselves were approx. 3–3.5 nm apart suggesting that these features are the side view of aligned rows of fibers. Such a periodic alignment would occur if the hexagonally packed bundles twisted about their center. In which case, as viewed from the side the rows would align with every 60° rotation and give the appearance of striations. For some circular structures, the striations appeared to persist. Perhaps the pitch of the rotation and the curvature were synchronized or perhaps there was some interaction with the inner monolayer that allowed alignment with that surface.

3.3. Small angle X-ray diffraction of DOX aggregates

X-Ray diffraction was used to better understand the packing details of the aggregates. Although we could not sufficiently concentrate liposomes for peak analysis by small angle X-ray diffraction (SAXS) we were able to examine the DOX-citrate aggregates pelleted via centrifugation. Fig. 3 shows the diffraction from samples produced at pH 4 and pH 5. The pH 4 material at room temperature showed similar

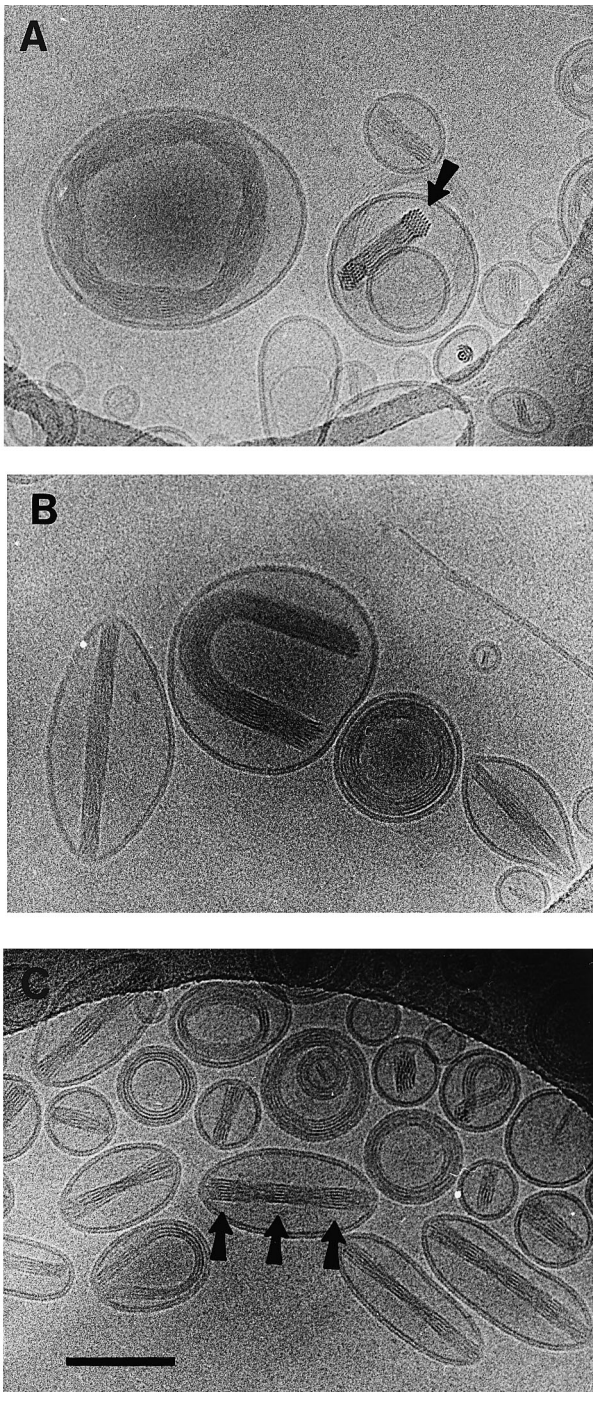

Fig. 2. Cryo-EM images (three fields) of DOX loaded into liposomes buffered by citrate. The final DOX solution concentration was 3.4 mM which is estimated to be 200–300 mM DOX internally. This internal concentration was estimated based upon DOX loading and the liposome captured volume (see Table 2). The total lipid concentration was 12.8 mM and the sample was undiluted for microscopy. The arrow in A indicates the end of a fibrous bundle in which the fibers are hexagonally arranged with an approx. 3–3.5 nm separation. In B, a circular, U-shaped, and straight DOX-citrate complex are noted. The arrows in C indicate striated regions in the DOX fibrous bundles with a repeating distance of approx. 50 nm. Bar represents 100 nm.
←

diffraction both before heating (Fig. 3A) and after a heating protocol (see Section 2.5) meant to mimic the temperature protocol used to load liposomes, e.g., heat briefly to 55–60°C and then cool back down to 20°C (data not shown). The arrows in Fig. 3A showed the expected peak positions of an oblique lattice of $a = 33.6$ Å, $b = 29.2$ Å, and $\gamma = 40°$, as obtained by a least squares fit of Eq. 5 to the data. Because of the paucity of diffraction peaks, and the absence of certain peaks (which may simply be too weak to be seen), the lattice assignment should be taken as possible, but not unequivocal. The pH 5 material, before heating, yielded diffraction very similar to the pH 4 material (data not shown). However, upon heating to 55–60°C and then cooling back to 20°C, the diffraction pattern changes to that seen in Fig. 3B. An unconstrained fit to Eq. 5 yields $a = 33.7$ Å, $b = 35.7$ Å, and $\gamma = 61.48°$. This is within the measurement errors of the simple hexagonal lattice (34.5 Å basis length), indicated by the arrows in the figure.

A weak peak corresponding to a real space repeat of 10.1 Å is also seen in the data, as shown in Fig. 3A (see the peak in between the ones indexed with (2,0) and (3,3) in the figure). This does not fit the planar lattice assignment and might be due to correlations along the direction of the fibers, that is to say perpendicular to the lattice plane.

From these data it would appear that doxorubicin-citrate fiber bundles can adopt two distinct packing arrangements. A simple hexagonal packing arose when both a pH 5 environment and a heating/cooling (recrystallization) step were employed for the unencapsulated solution fibers. These conditions may be met for liposomal DOX since the interior pH of the loaded vesicles increases to near pH 5 (see examples in Table 3) and, as per our protocol, liposomes are always heated during loading (see Section 2.3).

We tried to determine whether the oblique structure is present in the liposomes as well. As mentioned before, it was difficult to directly index peak posi-

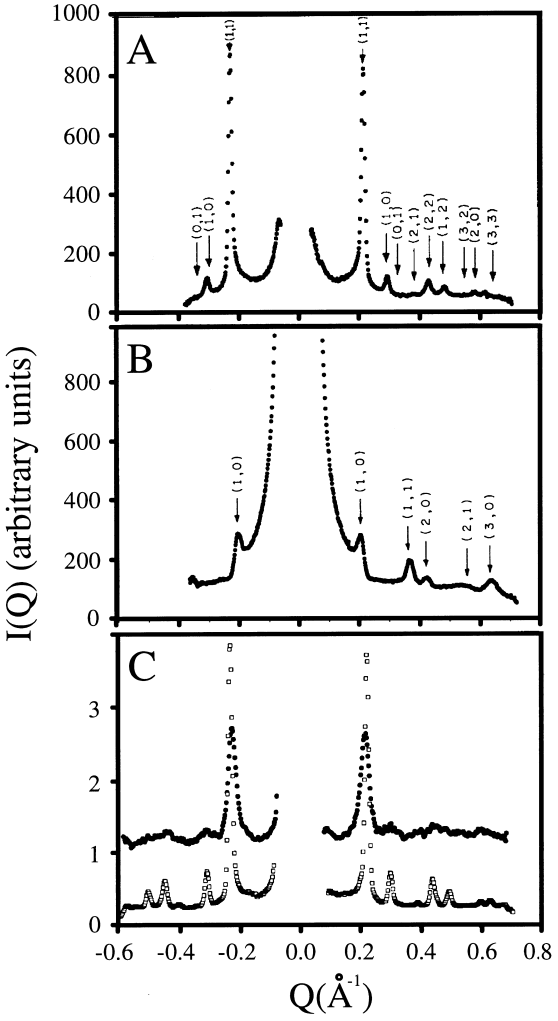

Fig. 3. Small angle X-ray diffraction patterns of DOX-citrate complexes in solution at (A) pH 4 and (B) pH 5 or in pelleted liposomes (C). For the pH 4 sample (A), the pattern is from an unheated sample: heating and cooling the sample did not appreciably change the diffraction pattern. The arrows show the expected peak positions for the oblique lattice described in the text. Diffraction from the samples at pH 5 before heating looked very similar to samples at pH 4, e.g., as shown in A. The pattern for pH 5 samples changed to that shown in B upon heating and cooling. The arrows show the expected peak positions for the hexagonal lattice described in the text. The upper pattern of C is that derived for the DOX-citrate complex inside loaded liposomes (see text for details). Shown for reference, the lower pattern of C is that for DOX-citrate complex pelleted from solution at pH 4.

tions for the DOX-citrate loaded liposomes – Fig. 3C (upper pattern) shows an example of the diffraction pattern of pelleted DOX loaded liposomes. Any signal arising from a DOX-citrate lattice in the liposomes would be superimposed on a signal arising from the liposome shells. Hence we adopted the following procedure: an image was taken of the DOX loaded liposomes as well as one of the empty liposomes (not shown). Assuming that the total scattering arises from the product of the liposome form factor and the structures factor arising from the DOX-citrate complex, we divided the diffraction from the DOX loaded liposomes by that of the empty liposomes (Fig. 3C, top pattern). Even with poor statistics, one can see that the resultant peaks coincide with those of the DOX-citrate complex formed in solution at pH 4 (lower pattern of Fig. 3C). This suggests that the oblique lattice may also be present in the liposomes. Note that the resolution of the cryo-EM images does not allow us to discriminate between a simple hexagonal lattice and a slightly skewed hexagonal lattice.

3.4. Circular dichroism of doxorubicin in liposomes

As expected, unentrapped DOX that was mixed with empty liposomes exhibited a CD pattern consistent with disaggregated dimeric DOX [35,36] (see Fig. 4). This spectrum was identical to that for

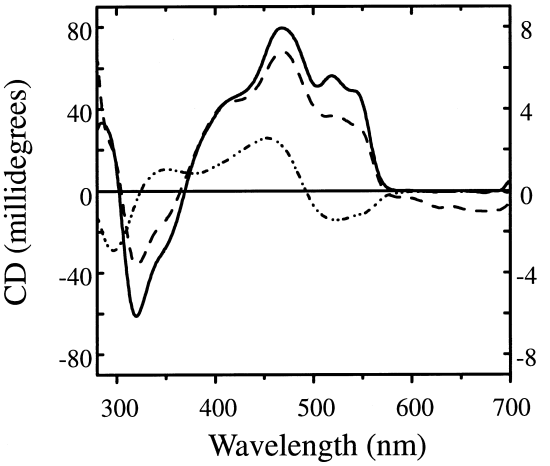

Fig. 4. CD spectra of DOX loaded into citrate containing liposomes via a pH gradient where the final DOX concentration was either 3.4 mM (solid line, left y-axis) or 0.34 mM (dashed line, right y-axis). Internal DOX concentrations were estimated to be 200–300 mM and 20–30 mM, respectively. Also shown is 3.4 mM DOX mixed with empty liposomes with no pH gradient (dotted-dashed line). Liposomes (approx. 100 nm LUVs) contained 300 mM citrate and lipid concentration was 12.8 mM.

DOX in water without liposomes (data not shown). Loading of DOX into citrate containing liposomes dramatically changed its CD spectrum (Fig. 4). The CD spectrum of loaded DOX indicated that a significant change in DOX interactions had occurred, consistent with the observed structure formation.

When DOX was loaded to a ten times lower concentration into liposomes the CD signal was nearly the same (see Fig. 4). As shown in Fig. 5, cryo-EM images of these loaded liposomes revealed similar internalized structures to those found in liposomes loaded to the ten times higher internal DOX concentration. The dimensions of the internal DOX structures were smaller in both length and breadth as compared to those of Fig. 2 with fewer fibers per bundle. Because of these images and because there seemed to be little contribution to the CD pattern from disaggregated DOX we believe the complexed form is the predominant DOX species inside citrate containing liposomes. In fact, for liposomes loaded to the higher internal concentration of DOX we estimate from analysis of CD spectra that the DOX-fiber species accounts for greater than 99% of the total DOX.

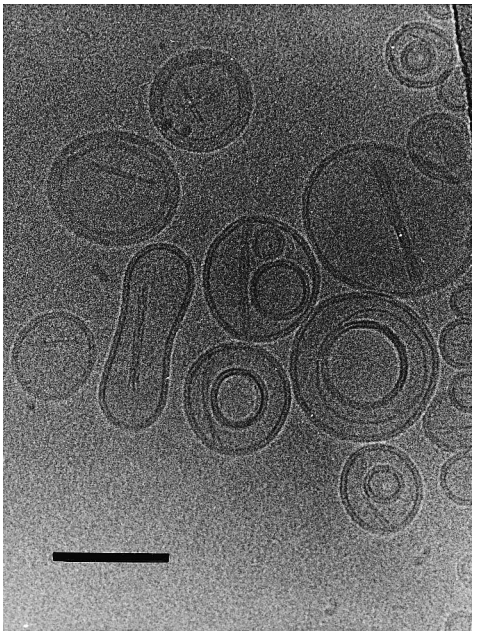

Fig. 5. Cryo-EM image of DOX loaded into citrate containing liposomes where the final DOX concentration was 0.34 mM. The internal DOX concentration was estimated to be 20–30 mM. The lipid concentration was 12.8 mM. Bar represents 100 nm.

3.5. Influence of citrate upon doxorubicin dimerization

To understand more about how citrate interacts with DOX we examined whether the citrate anion influences the association of DOX monomers into dimers. This association occurs at very low DOX concentrations in water (from 5 to 20 μM) and one might expect citrate to influence this conversion if the dimer is arranged such that the two positive charges from the sugar moieties can be bridged by the citrate multianion. We compared the CD spectra of DOX in either water or a solution of 300 mM citrate over the range of concentrations at which monomer to dimer conversion is expected (data not shown). At 5 μM DOX, CD spectra were similar to each other and to that previously reported for monomeric DOX and daunorubicin [35,36]. While there were changes from 5 μM to 1 mM that were consistent with monomer to dimer conversion [35–37], the spectra for DOX in water and citrate were similar to one another up to 1 mM DOX. However, at 2 mM DOX the CD patterns began to differ significantly, consistent with our assessment of aggregation by turbidity (Table 1). From these data it does not appear that citrate influences DOX dimerization. This might suggest that dimerized DOX molecules are oriented such that the cationic amines cannot be bridged by the citrate multianion. This finding, along with our other data, also suggests that citrate induces aggregation by coupling DOX dimers/oligomers (dimers into oligomers and/or oligomers into side-by-side packed fiber bundles).

3.6. ^{13}C-NMR measurements of citrate

To better understand the interactions between DOX and the citrate counterion inside liposomes, we used ^{13}C-NMR to examine internalized citrate. The terminal carboxylic acid carbons of citrate, carbons 1 and 5, are chemically identical and, at any particular pH, give rise to a single resonance in the ^{13}C-NMR spectrum. In our NMR studies of citrate buffered liposomes, the ^{13}C-NMR signal arising from the terminal carboxylic acid carbons was enhanced by the presence of [1,5-^{13}C]citrate. To simplify our description of the NMR results, we will refer to the resonance arising from these terminal carboxylic acid carbons as the citrate resonance.

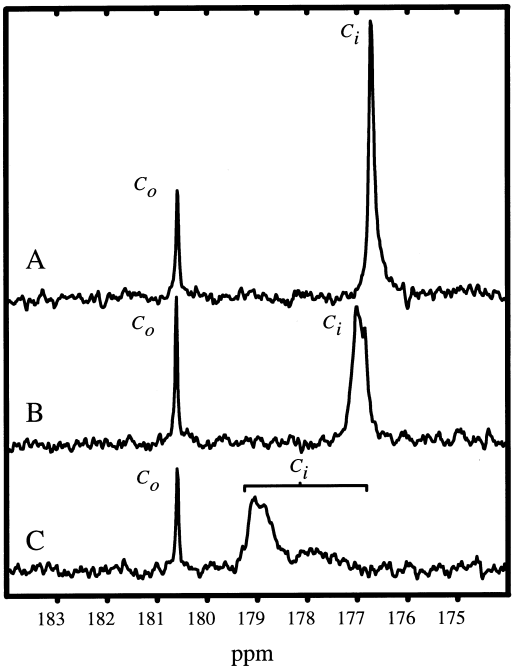

Fig. 6. Effect of DOX loading on the ^{13}C chemical shift and line width of the citrate resonance. ^{13}C-NMR spectra of EPC/cholesterol liposomes with an initial pH gradient created by 270 mM citrate, pH 4.0, inside and 20 mM HBS at pH 7.5 outside. After the exchange of external citrate buffer for 20 mM HBS, pH 7.0, some residual citrate remained outside the liposomes. This resonance is labeled C_o in the figure above. The resonance due to internal citrate is labeled C_i. Subsequent to creation of the pH gradient the liposomes were loaded with: (A) 0 mM, (B) 0.34 mM (20–30 mM internal concentration) and (C) 3.4 mM DOX (200–300 mM internal concentration). The lipid concentration was 12.8 mM. Internal pH values as determined from the chemical shifts were (A) pH 4.0, (B) pH 4.2–4.0, and (C) pH 5.5–4.1, consistent with the values of Table 3.

In citrate buffered liposomes, the citrate resonance from inside the liposome was shifted and broadened by the loading of DOX (Fig. 6). The chemical shifts observed are consistent with an increase in the internal pH of the DOX loaded liposomes (see Table 3). We believe that the broadening of the citrate resonance is due to a distribution of internal pH values within the liposomes, produced by DOX loading. The modest decrease in T_2 of the citrate resonance which occurs with DOX loading (Table 2) cannot account for the magnitude of the line broadening observed. In LBA buffered liposomes, loading with DOX induced similar changes in the chemical shift and line width of the resonance arising from the carboxylic acid carbon of internal LBA, (data not shown).

Because cryo-EM images show that DOX formed fibrous structures inside citrate buffered liposomes, one might expect that some fraction of the citrate would also be immobilized. If so, this citrate might not be observed in the solution state spectrum due to lifetime broadening or dipolar broadening of its resonance. Assuming a charge ratio of 3:1, citrate to DOX, and complete loading of the DOX into the liposomes, one would expect that approx. 18% of the citrate would be associated with DOX through electrostatic interactions alone. However, the signal intensity from citrate is, to within the uncertainty in our measurement, unchanged by the loading of DOX (approx. 200 mM inside) (Table 2). What we do observe is a modest decrease in the T_1 and T_2 of the citrate signal (Table 2), suggesting that citrate 'bound' to DOX fibers may be in rapid exchange with 'free' citrate.

3.7. LBA liposomes

The DOX structures inside liposomes that formed with citrate were similar in appearance to those formed with the divalent sulfate anion [13]. To determine whether these internalized DOX structures required a multivalent counterion in order to form, we next examined liposomes loaded with DOX using the monoanionic buffer LBA to control pH; the initial internal pH was approx. 4 and the outside pH was raised to approx. 7.4. Cryo-EM of LBA liposomes containing DOX at internal concentrations

Table 2
T_1, T_2, and normalized intensity of the ^{13}C resonance from [1,5-^{13}C]citrate inside liposomes

[DOX] (mM)	T_1 (s)	T_2 (s)	Normalized intensity[a]
0.0	6.1 ± 0.5	0.16 ± 0.03	–
0.34	4.9 ± 0.2	–	–
3.4	2.6 ± 0.4[b] 4.5 ± 1.0	0.09 ± 0.03[c]	1.01 ± 0.08[c]

[a]Intensities were normalized to that of citrate with 0 mM DOX.
[b]The internal citrate gave rise to two broad resonances in these liposomes. The first T_1 corresponds to the more 'downfield' peak.
[c]These numbers reflect the integrated area of both resonances.

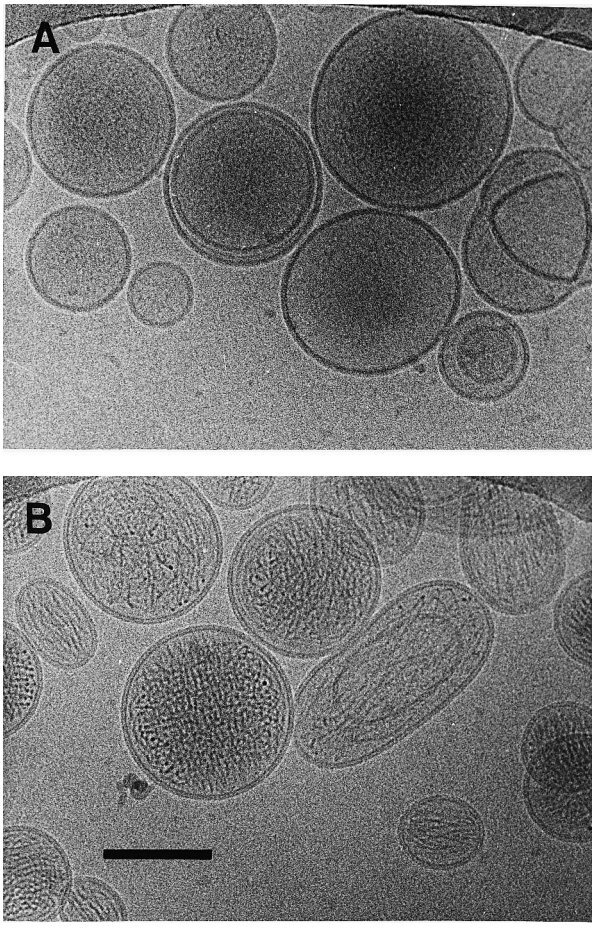

Fig. 7. Cryo-EM images of DOX loaded into liposomes buffered by LBA. (A) Liposomes contained LBA (650 mM) as buffer and the solution concentration of DOX was 0.34 mM, which would give an internal [DOX] of approx. 20–30 mM. (B) LBA liposomes loaded such that the final solution concentration of DOX was 3.4 mM, which we estimate to be 200–300 mM DOX internally. The lipid concentration was 12.8 mM and samples were examined undiluted for microscopy. Bar represents 100 nm.

of 20–30 mM DOX did not reveal any noticeable structures (Fig. 7A); an occasional fiber was the exception. Again no membrane invagination was noted. The CD pattern for DOX loaded into LBA liposomes at this low concentration was consistent with disaggregated dimeric DOX (Fig. 8). At internal DOX concentrations of approx. 200–300 mM, far in excess of DOX's solubility limit, what appeared to be numerous uncondensed fibers were observed in the liposomes (Fig. 7B). The CD pattern for these uncondensed DOX fibers was similar to that for DOX fiber bundles in citrate bearing liposomes except that the shoulder at 520 nm was decreased relative to the other peaks (Fig. 8); this shoulder could be sensitive to 'side-by-side fiber' interactions.

Apparently, DOX fiber formation occurs in LBA liposomes only at DOX concentrations in excess of its aqueous solubility limit, which you will recall is approx. 60 mM in water [12]. LBA is incapable of bridging charges so the fibers that formed above the solubility limit of DOX remained uncondensed. This implies that the DOX fiber bundles observed inside citrate containing liposomes are the result of the citrate multianion electrostatic bridging between separate fibers. Although citrate may have simply eliminated charge repulsion, thus allowing an otherwise favorable association to occur, this seems less likely to be the reason for condensation since LBA could have also served this purpose but did not.

3.8. *Effect of DOX physical state upon liposomal release*

Having established that the DOX aggregation state inside the liposome can be manipulated, we next ventured to make comparable liposomes containing either citrate or LBA to establish the effect of DOX's physical state upon the release rate. The physical properties of these liposomes are listed in Table 3. Liposomes contained either 650 mM LBA

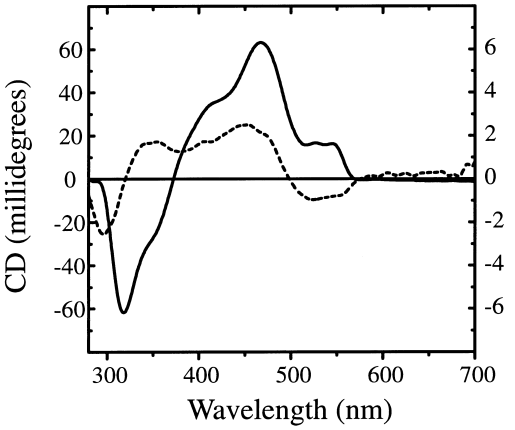

Fig. 8. CD spectra of DOX loaded into liposomes containing LBA as buffer. Final solution DOX concentrations were 3.4 mM (solid lines, left y-axis) or 0.34 mM (dashed lines, right y-axis). The final lipid concentration was 12.8 mM. For the lower concentration of DOX in LBA liposomes, the CD signature indicated that DOX was predominantly disaggregated dimers.

or 300 mM citrate, both at pH approx. 4 initially, and were loaded to low (16–29 mM) or high (160–290 mM) internal concentrations of DOX. (For LBA, 650 mM was required to achieve complete DOX loading; 500 mM LBA was insufficient (not shown).) The liposomes were diluted into hepes buffered saline and leak monitored as described in Section 2.3.

In all cases where the internalized DOX formed fibers, the leak profiles were indistinguishable with less than approx. 4% leak after 60 min (data not shown). For those LBA liposomes in which DOX was loaded to a low internal concentration (no fibers), the leak profiles were biphasic and variable with, in some cases, a significant loss of material in the first few minutes (see leak values at 10 min – Table 3).

When samples were diluted into a hyperosmotic (approx. 1060 mOsM) solution of buffer containing 20% (w/v) sucrose the liposomes displayed similar leak profiles ($<4\%$ leak at 60 min) for all four systems of Table 3 (fibers and no fibers) (data not shown). This indicated that osmotic stress was involved for the LBA containing liposomes with a low internal DOX concentration (no fibers). This was not too surprising since the expected osmotic differential for the LBA containing liposomes diluted into hepes buffered saline is approx. 565 mOsM which is close to the rupture threshold differential of 600 mOsM reported by Mui et al. [38] for spherical EPC/cholesterol liposomes of similar size and composition. Considering this, the variability in leak for DOX from LBA containing liposomes (no fibers) was not too surprising either since those liposomes may have been teetering on the threshold amount of stress required to cause rupture.

The reason why DOX leak from the LBA liposomes loaded to a high DOX internal concentration (fibers) did not also display a rapid component is unclear, but in those liposomes DOX did form fibers that may have been restricted sterically from escaping the vesicle. Alternatively, it may be that only the LBA liposomes containing the lower amount of disaggregated-DOX were osmotically stressed. That is, the cationic DOX fibers that formed at higher DOX internal concentrations may have bound a significant portion of the LBA molecules, and thus reduced the osmotic difference.

Table 3
Properties of loaded liposomes

Buffer	Physical state of DOX inside	[DOX] (mM)	Internal [DOX] (mM)	Cap. volume (μl/μmole)	Mean vesicle size (nm)	Final ΔpH	Internal pH	% leak at 10 min
Citrate	fibers (bundles)	3.4	290	0.9	124	2.5	4.9	0.8
		3.4	290	0.9	99	1.8	5.6	1.1
	fibers (bundles)	0.34	29	0.9	124	2.9	4.7	0.7
		0.34	29	0.9	124	–	–	0.1
		0.34	29	0.9	99	2.6	4.6	0.1
		0.34	29	0.9	99	2.6	4.8	0.1
LBA	fibers	3.4	260	1.0	120	1.0	6.4	0.8
		3.4	250	1.1	120	0.6	6.8	0.1
		3.4	160	1.6	94	2.4	5.0	<0.1
		3.4	200	1.3	115	2.4	5.0	1.3
	no fibers	0.34	24	1.1	120	2.4	5.0	1.3
		0.34	16	1.6	94	3.2	4.2	1.7
		0.34	16	1.6	94	3.2	4.2	0.5
		0.34	20	1.3	115	3.1	4.3	13.1
		0.34	20	1.3	115	–	–	18.4
		0.34	20	1.3	115	3.1	4.3	9.7

Liposomes were made in either 300 mM citrate or 650 mM LBA at pH 4. Vesicle sizes, captured volumes, and pH measurements were performed as outlined in Section 2. The listed DOX concentrations were the overall solution values prior to dilution; internal concentrations were estimated based on captured volume, lipid concentration, and loading efficiency (for all cases $>95\%$) (see text). ΔpH and internal pH values were determined for vesicles following DOX loading. Leakage experiments were performed immediately after DOX loading (<1 h) and the data represent the percent leakage at the 10 min point along the leak curves (not shown) for samples diluted into HEPES buffered saline.

4. Discussion

In solution, citrate, like sulfate, caused DOX aggregation to occur at concentrations 100 times lower than its aqueous solubility limit. Inside citrate containing liposomes, DOX loaded via a pH gradient was found to exist in fiber bundles by cryo-EM with no observable membrane invagination. While the straight fiber bundles were somewhat similar in appearance to the DOX-sulfate aggregates observed by Lasic and co-workers [12,39], we also noted curved and circular fiber bundles. These appeared to result from the bending of the linear structures that had grown in length beyond what the liposome was capable of accommodating. End-on views of these DOX-citrate fiber bundles indicated that the fibers were packed longitudinally in a hexagonal arrangement with a separation of approx. 3–3.5 nm between fibers. Two distinct diffraction patterns were also observed by SAXS for DOX-citrate fiber bundles in solution, an oblique and a simple hexagonal lattice. Which of the two, or if both, are present inside liposomes remains unclear since cryo-EM does not have the resolution to distinguish between a simple hexagonal and a slightly skewed hexagonal packing. Even so the basis lengths noted by SAXS likely correspond to the interfiber distance estimated by cryo-EM, both approx. 30–35 Å. The repeating striations observed for fiber bundles suggests that the entire bundle twists 60° approximately every 50 nm. This is consistent with a twisting hexagonal lattice since, as viewed from the side, the rotation of a hexagonal array affords spatial alignment every 60° (see Fig. 9). The fact that the peaks of Fig. 3B do not correspond exactly to a hexagonal pattern may be consistent with our assumption that we have a slightly tilted hexagonal structure that is twisting.

Because for DOX-sulfate aggregates only straight bundles (rods) were noted by cryo-EM [12,13], the appearance of curved and circular bundles here would seem to indicate that our DOX-citrate fiber bundles are more flexible. Since only individual fibers formed in LBA liposomes (Fig. 2B) we believe that bundles formed in citrate containing liposomes due to interfiber crosslinking by the citrate multianion. This would then suggest that the difference between

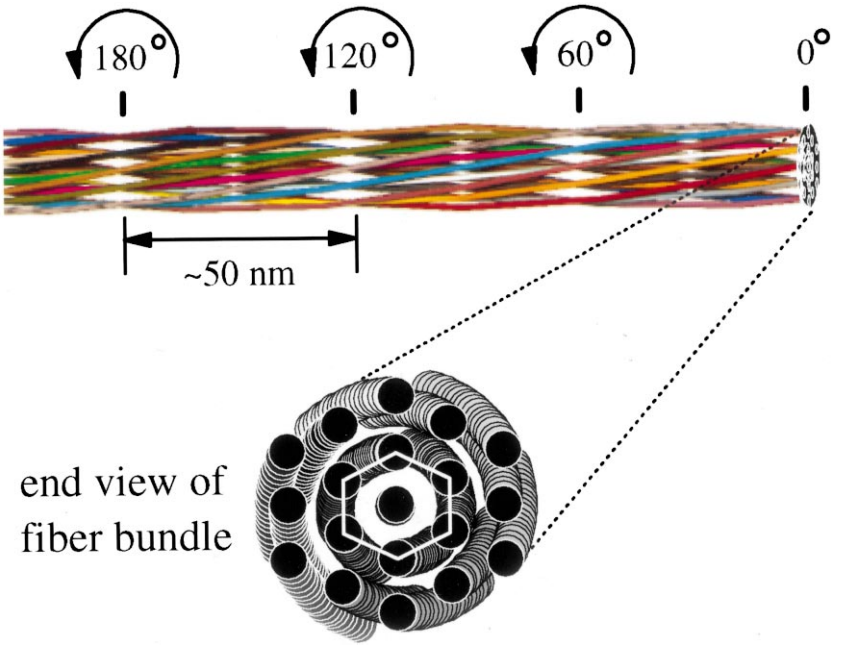

Fig. 9. Schematic representation of twisting hexagonally arranged fibers. In this proposed model each fiber is comprised of stacked DOX molecules. The lower illustration depicts how the stacked DOX molecules (circles) would appear as viewed end-on. As viewed from the side (upper illustration), the fibers are aligned along the line of sight at rotation multiples of 60° thus giving the appearance of repeating striations. For an oblique lattice, the interfiber distance across each striated zone would vary. This variation might not be resolvable in the cryo-EM images if the obliquity is only slightly different from hexagonal, as seems to be the case here, based on SAXS results.

DOX-sulfate and DOX-citrate fiber bundles stems directly from differences in the counterions themselves. Although the interfiber spacing for DOX-citrate aggregates was 30–35 Å the separation noted for DOX-sulfate fibers was reported to be approx. 27 Å [12]. This tighter packing is consistent with the fact that sulfate is a smaller ion. Additionally, fiber flexibility may also involve differences in the multianion's binding affinity. Although we have no sense of sulfate binding we did find here from NMR experiments with ^{13}C-citrate that the citrate-DOX interaction was quite dynamic with rapid exchange of 'free' and 'bound' citrate.

We have not detailed how DOX forms fibers but given its planar structure it seems likely that DOX molecules stack. Because citrate did not affect monomer to dimer conversion one might argue that the amino sugar moieties are separated far enough that citrate could not bridge/couple monomers. Interestingly, upon stacking/ aggregating porphyrins exhibit a significantly increased scattering intensity at the absorption wavelengths; this phenomenon has been termed resonance light scattering (RLS) [26,27,40]. In our hands, the DOX fibrous structures did not exhibit RLS (data not shown). This result, though not conclusive, may indicate that RLS is a specific phenomenon of the large porphyrin ring systems.

For DOX loaded into liposomes containing the monoanionic buffer LBA, its physical state was dependent upon the internal DOX concentration.

When loaded to only approx. 20 mM DOX, there were no discernible structures inside LBA liposomes and the CD pattern was consistent with disaggregated DOX. It is quite interesting that this CD pattern was identical to that for dimeric and not monomeric DOX because Gallois et al. [36] using CD have reported that DOX partitioned onto large unilamellar vesicles (LUVs) was monomeric and not dimeric. While this might suggest that no binding of DOX to the membrane occurred we cannot rule out that for our liposomes DOX binds to the membrane surface as the dimeric species. In any case, no membrane invagination was noted.

When loaded into LBA liposomes at high internal concentrations DOX formed fibers. Again no membrane invagination was noted by cryo-EM. Unlike the DOX in citrate containing liposomes, these fibers were disorganized and not condensed into bundles (Fig. 8B). Apparently DOX stacking to form fibers occurs above its solubility limit regardless if whether there is a multivalent counterion present or not. These results with LBA would also seem to confirm that the fiber bundles in citrate containing liposomes arise because the citrate multianion facilitates interfiber crosslinking.

Interestingly, this crosslinking of fibers by citrate did not dramatically slow the rate of DOX release as it was similar to that for DOX out of LBA liposomes where the DOX was disaggregated. From ^{13}C-NMR experiments it was apparent that 'bound' DOX was in rapid exchange with 'free' DOX. Such a dynamic relationship would be consistent with the unhindered leak of DOX from the citrate containing liposomes. However, because liposome integrity/stability is a major concern in vivo, fiber formation (and fiber bundles in particular) may enhance the stability of DOX loaded liposomes by providing a possible steric hindrance to vesicle rupture. It has been shown that lipoprotein adsorption onto PC/cholesterol LUVs significantly decreased their ability to withstand osmotic stress [41]. Consequently, liposomes with uncomplexed DOX may leak more significantly in vivo (work now underway).

Cullis and co-workers proposed that DOX is predominantly bound to the inner monolayer [14] and that this binding leads to an invagination of the membrane [15]. From the work presented here it is obvious that citrate produced organized aggregated DOX-citrate structures inside liposomes. Also obvious from our cryo-EM images is that membrane morphology is unaffected by DOX loading. The conclusion by Cullis and co-workers that membrane invagination occurred was based upon less well resolved cryo-EM images (DOX liposomes looked like 'coffee beans') where the DOX-citrate fiber aggregates appeared as blurred lines inside the liposomes which could be mistaken for a membrane edge [15]. To discard any possibility that DOX from different vendors might yield a different interaction, we examined three different DOX vendor materials (one which included methyl paraben and two that did not) and found identical structures inside liposomes (data not shown). Cullis and co-workers found that DOX's ^{13}C-NMR signal was significantly broadened when internalized in citrate bearing liposomes [14]. While they interpreted this as due to

inner monolayer binding, our data clearly indicate that the explanation for this molecular immobilization is caused by DOX complexation with citrate. As we have demonstrated here, packing of adjacent DOX fibers into bundles was facilitated by citrate which lowered the solubility limit of DOX significantly. Although we cannot rule out that some DOX may be partitioned into the inner monolayer, we believe that this DOX accounts for only a small percentage of the total internalized DOX.

Acknowledgements

This work was supported by the Liposome Company, Inc. We thank Dr. Eric Mayhew for his assistance performing the confocal microscopy, Dr. Robert Pasternack for a fruitful discussion of resonance light scattering, and Rao Fu for help creating Fig. 9 color graphic. X-Ray instrumentation development in SMG's lab is supported by the Dept. of Energy (DEFG02-97ER624434).

References

[1] J.G. Hardman, L.E. Limbird (Eds.-in-Chief), Goodman and Gilman's The Pharmacological Basis of Therapeutics, 9th edn., McGraw-Hill, New York, 1996, p. 1265.
[2] J.A.E. Balazsovits, L.D. Mayer, M.B. Bally, P.R. Cullis, M. McDonell, R.S. Ginsberg, R.E. Falk, Cancer Chemother. Pharmacol. 23 (1989) 81–86.
[3] F. Olson, E. Mayhew, D. Maslow, Y. Rustum, F. Szoka, Eur. J. Cancer. Clin. Oncol. 18 (1982) 167–176.
[4] A. Gabizon, A. Meshorer, Y. Barenholz, J. Natl. Cancer Inst. 77 (1986) 459–469.
[5] P.M. Kanter, G.A. Bullard, R.A. Ginsberg, F.G. Pilkiewicz, L.D. Mayer, P.R. Cullis, Z.P. Pavelic, In Vivo 7 (1993) 17–26.
[6] G.A. Fonseca, V. Valero, A. Buzdar, R. Walters, J. Wiley, R. Benjamin, M. Ewer, B. Mackay, D. Gordon, G. Hortobagyi, Proc. 31st Annual Meeting Am. Soc. Clin. Oncol., 20–23 May 1995, abstr. 95, p. 99.
[7] T.D. Madden, P.R. Harrigan, L.C.L. Tai, M.B. Bally, L.D. Mayer, T.E. Redelmeier, H.C. Loughrey, C.P.S. Tilcock, L.W. Reinish, P.R. Cullis, Chem. Phys. Lipids 53 (1990) 37–46.
[8] L.D. Mayer, M.B. Bally, M.J. Hope, P.R. Cullis, Biochim. Biophys. Acta 816 (1985) 294–302.
[9] G. Haran, C. Rivka, L.K. Bar, Y. Barenholz, Biochim. Biophys. Acta 1151 (1993) 201–215.
[10] A. Vigevani, M.J. Williamson, in: K. Florey (Ed.), Analytical Profiles of Drug Substances, vol. 9, Academic Press, New York, 1980, pp. 245–274.
[11] L.D. Mayer, L.C.L. Tai, M.B. Bally, G.N. Mitilenes, R.S. Ginsberg, P.R. Cullis, Biochim. Biophys. Acta 1025 (1990) 143–151.
[12] D.D. Lasic, P.M. Frederik, M.C.A. Stuart, Y. Barenholz, T.J. McIntosh, FEBS Lett. 312 (1992) 255–258.
[13] D.D. Lasic, B. Ceh, M.C.A. Stuart, L. Guo, P.M. Frederik, Y. Barenholz, Biochim. Biophys. Acta 1239 (1995) 145–156.
[14] P.R. Harrigan, K.F. Wong, T.E. Redelmeier, J.J. Wheeler, P.R. Cullis, Biochim. Biophys. Acta 1149 (1993) 329–338.
[15] P.R. Cullis, M.J. Hope, M.B. Bally, T.D. Madden, L.D. Mayer, D.B. Fenske, Biochim. Biophys. Acta 1331 (1997) 187–211.
[16] M.B. Bally, R. Nayar, D. Masin, M.J. Hope, P.R. Cullis, L.D. Mayer, Biochim. Biophys. Acta 1023 (1990) 133–139.
[17] F. Frezard, J. Liposome Res. 4 (1994) 1063–1073.
[18] S.M. Gruner, R.P. Lenk, A.S. Janoff, M.J. Ostro, Biochemistry 24 (1985) 2833–2842.
[19] W.R. Perkins, S.R. Minchey, M.J. Ostro, T.F. Taraschi, A.S. Janoff, Biochim. Biophys. Acta 943 (1988) 103–107.
[20] P.S. Chen Jr., T.Y. Toribara, H. Warner, Anal. Chem. 28 (1956) 1756–1758.
[21] M.J.H. Janssen, D.J.A. Crommelin, G. Storm, A Hulshoff, Int. J. Pharm. 23 (1985) 1–11.
[22] R.J. Mehlhorn, L. Packer, R. Macey, T. Alexandru, I. Dragutan, Methods Enzymol. 127 (1986) 738–745.
[23] W.R. Perkins, S.R. Minchey, P.L. Ahl, A.S. Janoff, Chem. Phys. Lipids 64 (1993) 197–217.
[24] K. Anzai, M. Yoshida, Y. Kirino, Biochim. Biophys. Acta 1021 (1990) 21–26.
[25] M.W. Tate, S.M. Gruner, E.F. Eikenberry, Rev. Sci. Instr. 68 (1997) 47–54.
[26] R.F. Pasternack, C. Bustamante, P.J. Collings, A. Giannetto, E.J. Gibbs, J. Am. Chem. Soc. 115 (1993) 5393–5399.
[27] J.C. de Paula, J.H. Robblee, R.F. Pasternack, Biophys. J. 68 (1995) 335–341.
[28] L.D. Mayer, M.B. Bally, P.R. Cullis, Biochim. Biophys. Acta 857 (1986) 123–126.
[29] C.L. Shapiro, T. Ervin, N. Azamia, J. Keating, V. Suppers, L. Ayash, D. Hayes, and the D99-Study Group, Programs/Proceedings of the 32nd Annual Meeting of the American Society of Clinical Oncology, Philadelphia, PA, May 18–21 1996, abstr. 115.
[30] E. Early, S. Shorter, A. Sugarman, G.K. Schwartz, J. Woodruff, M.F. Brennan, E.S. Casper, Programs/Proceedings of the 32nd Annual Meeting of the American Society of Clinical Oncology, Philadelphia, PA, May 18–21 1996, abstr. 1690.
[31] E.S. Casper, G.K. Schwartz, A. Sugarman, D. Leung, M.F. Brennan, J. Clin. Oncol. 15 (1997) 2111–2117.
[32] J.-H. Fuhrlop, J. König, Membranes and Molecular Assemblies: the Synkinetic Approach, Royal Society of Chemistry, Cambridge, 1994, pp. 126–139.

[33] H. Matsuki, R. Ichikawa, S. Kaneshina, H. Kamaya, I. Ueda, J. Colloid Interface Sci. 181 (1996) 362–369.
[34] H. Satake, H. Matsuki, S. Kaneshina, Coll. Surf. A Physicochem. Eng. Asp. 71 (1993) 135–140.
[35] A. Garnier-Suillerot, L. Gattegno, Biochim. Biophys. Acta 936 (1988) 50–60.
[36] L. Gallois, M. Fiallo, A. Garnier-Suillerot, Biochim. Biophys. Acta 1370 (1998) 31–40.
[37] N. Henry-Toulme, B. Stefanska, E. Borowski, J. Bolard, Mol. Pharmacol. 33 (1988) 574–579.
[38] B.L.-S. Mui, P.R. Cullis, E.A. Evans, T.D. Madden, Biophys. J. 64 (1993) 443–453.
[39] D.D. Lasic, Nature 380 (1996) 561–562.
[40] R.F. Pasternack, P.J. Collings, Science 269 (1995) 935–936.
[41] B.L.-S. Mui, P.R. Cullis, P.H. Pritchard, T.D. Madden, J. Biol. Chem. 269 (1994) 7364–7370.